Dear Author,

Please, note that changes made to the HTML content will be added to the article before publication, but are not reflected in this PDF.

Note also that this file should not be used for submitting corrections.

Acta Materialia xxx (2015) xxx–xxx

Contents lists available at ScienceDirect

Acta Materialia

journal homepage: www.elsevier.com/locate/actamat

Chemical stability of $YBiO_3$ buffer layers for implementation in $YBa_2Cu_3O_{7-\delta}$ coated conductors

Glenn Pollefeyt [a], Alexander Meledin [b], Cornelia Pop [c], Susagna Ricart [c], Ruben Hühne [d], Gustaaf Van Tendeloo [b], Isabel Van Driessche [a,*]

[a] SCRiPTS, Dep. of Inorganic and Physical Chemistry, Ghent University, Krijgslaan 281-S3, 9000 Ghent, Belgium
[b] EMAT, Dep. of Physics, University of Antwerp, Groenborgerlaan 171, 2000 Antwerp, Belgium
[c] CSIC-ICMAB, Campus UAB, Bellaterra, Spain
[d] Institute for Metallic Materials, IFW Dresden, 01069 Dresden, Germany

ARTICLE INFO

Article history:
Received 30 June 2015
Revised 3 August 2015
Accepted 12 August 2015
Available online xxxx

Keywords:
Coated conductors
High resolution electron microscopy
Superconductivity
Thin film coating

ABSTRACT

In this work, the chemical and microstructural stability of $YBiO_3$ buffer layers during the growth of $YBa_2Cu_3O_{7-\delta}$ (YBCO) was studied. The superconducting YBCO films were deposited via both Pulsed Laser Deposition as well as Chemical Solution Deposition. Although excellent superconducting properties are obtained in both cases, self-field critical current densities of 3.6 and 1.2 MA/cm^2 respectively, chemical instability of the $YBiO_3$ buffer layer is observed. An elaborate transmission electron microscopy study showed that in the case of vacuum deposited YBCO, the $YBiO_3$ becomes unstable and Bi_2O_3 sublimates out of the architecture. Due to this structural instability, an intermediate Y_2O_3 layer is obtained which maintains it microstructural orientation relation with the substrate and acts as growth template for YBCO. For chemical solution deposited YBCO, reaction of YBCO with the $YBiO_3$ buffer layer is observed, leading to large grains of YBa_2BiO_6 which are pushed towards the surface of the films and strongly reduce the superconducting properties. Upon using high growth temperatures for the superconducting layer, these secondary phases decompose, which subsequently leads to Bi_2O_3 sublimation and a textured YBCO film which directly nucleated onto the $LaAlO_3$ single crystal substrate. Hence, this electron microscopy study indicates that bismuth-based buffer layers systems are not suitable for implementation in coated conductors.

1. Introduction

During the last decade, research in the field of superconductivity has been aiming for low-cost processing of $YBa_2Cu_3O_{7-\delta}$ coated conductors together with long length scalability in order to meet the requirements for main stream usage in power applications [1–3]. In this regard, Chemical Solution Deposition (CSD) of coated conductors is emerging as the leading deposition technique over the well-established vacuum deposition techniques [3–5]. The coated conductor design consists of a textured or polycrystalline metallic substrate, a stack of textured buffer layers and a textured superconducting YBCO film covered with a protective layer [4,6]. The use of one or more buffer layers is inevitable as they form a diffusion barrier between the substrate and the superconducting film, avoiding oxidation of the substrate and poisoning of the superconductor by metal-ions during thermal processing [2,4]. Due to the strong texture dependence of the critical current density J_c, these buffer layers have to be highly biaxially textured in order to allow the epitaxial growth of superconducting films on top [4,7]. Currently, the best results for CSD-based coated conductors have been obtained by using a double layered $La_2Zr_2O_7/CeO_2$ buffer architecture [8]. However, this architecture shows some potential drawbacks. First of all, state-of-the-art chemical solution deposited lanthanum zirconate is known to exhibit nanoporosity throughout the film [9,10]. The origin of this nanovoid formation is not well understood and is ascribed to either the removal of carbon gases during the synthesis or is believed to be an intrinsic characteristic of pyrochlore materials processed in reducing atmospheres [9–11]. Due to this porosity, both metal and oxygen diffusion are facilitated, which can lead to delamination of the complete architecture or an overall decrease in superconducting properties [7,11,12]. Secondly, the superconducting performance of the LZO/CeO_2 based coated conductors is hampered by the limited chemical stability of the CeO_2 buffer layer towards YBCO, leading to the formation of $BaCeO_3$ during thermal processing of the YBCO layer [13,14].

* Corresponding author.
E-mail address: isabel.vandriessche@ugent.be (I. Van Driessche).

http://dx.doi.org/10.1016/j.actamat.2015.08.023
1359-6454/

As an alternative buffer material, $YBiO_3$ (YBO) shows very interesting characteristics and properties. Its face centered cubic structure with a lattice constant of 0.5412 nm, results in an excellent lattice match with YBCO (0.2% mismatch with a_{YBCO} and 1.4% mismatch with b_{YBCO}) [15]. Furthermore, due to the low melting point of bismuth oxide (825 °C) a partial melting process is obtained during thermal processing, leading to the formation of a dense and smooth $YBiO_3$ layer at temperature of around 750 °C [16]. This topographical flatness in combination with a well maintained texture up to the surface of the film creates a favorable template for subsequent YBCO nucleation and growth [17,18]. We have previously shown that $YBiO_3$ buffer layers can be grown epitaxially on single crystal $LaAlO_3$ substrates by an aqueous chemical solution method [16]. YBCO deposition via Pulsed Laser Deposition (PLD) on these YBO-buffered single crystals yielded outstanding superconducting performances of 3.6 MA/cm^2. In this paper, the chemical stability and morphological properties of the $YBiO_3$ buffer layer after YBCO deposition via both PLD and low fluorine metal organic deposition (LF-MOD) are examined via X-ray diffraction analysis and electron microscopy.

2. Experimental

2.1. Solution preparation and growth

The detailed preparation of the aqueous $YBiO_3$ precursor solution has been described elsewhere [16]. Briefly, bismuth-citrate (Alfa Aesar, 94%) and yttrium acetate (Alfa Aesar, 99.9%) were dissolved in water by the addition of triethanolamine (Sigma–Aldrich, 99%) and ethanolamine (Sigma–Aldrich 99%). A 0.75 mol/L solution with neutral pH is obtained which exhibits a long shelf life. Thin $YBiO_3$ films were grown on polished (100) $LaAlO_3$ single crystal (CrysTec GmbH). Prior to dip-coating, the substrates were rinsed with isopropanol and heated to 400 °C for removing adsorbed organics [19]. After cooling the substrates to room temperature, dip-coating was performed with a withdrawal speed of 10 mm/min in a class 1000 clean room facility. The as-coated films were dried on a hot plate at 200 °C for 10 min. The high temperature synthesis was performed in a quartz tube furnace under a humid argon atmosphere, obtained by passing the Ar gas through two water bubblers at room temperature. The dried films were heated with 20 °C/min to 750 °C and dwelled at this temperature for 2 –4 h. The flow of the humid argon gas was kept constant at 150 mL/min for all performed experiments.

PLD-YBCO deposition was performed at a temperature of 810 °C and an oxygen background pressure of 0.3 mbar [20]. A KrF excimer laser was used, applying 3000 pulses on the YBCO target with a repetition rate of 5 Hz to deposit a 200 nm thick film. The samples were cooled down and oxygenated in an oxygen partial pressure of 0.4 bar. For the low fluorine MOD, YBCO precursor solutions were synthesized according to the procedures previously reported by Obradors et al. [21]. Yttrium trifluoroacetate, barium acetate and copper acetate are typically dissolved in a mixture of methanol, propionic acid and triethanolamine. The solutions were spin-coated onto the $YBiO_3$-buffered $LaAlO_3$ single crystals and subsequently calcined at 350 °C under humid O_2 atmosphere with a heating rate of 5 °C/min. The calcined layers were then crystallized at 780, 810 or 820 °C for 150 min under a humid 200 ppm O_2/N_2 atmosphere. After an additional dwell in dry processing conditions of 30 min, the YBCO films were annealed at 450 °C for 210 min in pure oxygen.

2.2. Microstructural characterization

Characterization of the texture and phase composition of the $YBiO_3$ and YBCO films was performed by means of X-ray diffraction (Siemens D5000 and Bruker GADDS D8 diffractometer). Structural characterization was carried out with both SEM (FEI Nova 600 Nanolab Dual Beam) and TEM. For the TEM measurements, cross-sectional lamellae were produced by Focused Ion Beam (FIB-SEM, FEI Nova 600 Nanolab Dual Beam and FEI Helios Dual Beam) and studied by conventional bright field transmission electron microscopy (BFTEM), bright field scanning transmission electron microscopy (BF-STEM) and energy dispersive X-ray spectroscopy (EDX) on a JEOL JEM 2200-FS operating at 200 keV. High angle annular dark field scanning transmission electron microscopy (HAADF-STEM) and EDX measurements were performed on a FEI Titan "cubed" electron microscope, equipped with an aberration corrector for the probe-forming lens as well as a high-brightness gun and a "Super-X" wide solid angle EDX detector, operating at 120 keV and on the FEI Osiris electron microscope equipped with a high-brightness gun and a "Super-X" wide solid angle EDX detector operating at 200 keV. The quality of the deposited YBCO layers was determined via inductive measurements of the critical temperature T_c and the critical current density J_c (Cryoscan™ by Theva and Quantum Design SQUID DC Magnetometer).

3. Results and discussion

3.1. Pulsed Laser Deposition of YBCO

The deposited YBCO exhibits a critical temperature $T_{c,90}$ of 90.4 K and a ΔT_c of 0.85 K. The $YBCO^{PLD}/YBO^{CSD}/LAO$ architecture yields outstanding superconducting properties with a critical current density of 3.6 MA/cm^2, indicating excellent texture transfer from the buffer layer to the superconducting layer [16].

The texture analysis of the $YBCO^{PLD}/YBO^{CSD}/LAO$ architecture is shown in Fig. 1. The φ-scan of the $YBa_2Cu_3O_{7-\delta}$ (102) reflection gives rise to a FWHM-value of 1.6°, indicating low in-plane misorientation. From the XRD measurement, it can be seen that no *a*-axis formation occurred. However, when comparing the (002) reflections of the buffer layer prior and post YBCO deposition, a shift towards higher Bragg angles is observed. Additionally, the intensity of the (110) reflection increases and also shifts to higher 2θ values. The Bragg angles for both reflections now coincide with the cubic Y_2O_3 crystal structure, which thus indicates that Bi^{3+} is eliminated from the buffer layer during Pulsed Laser Deposition of YBCO. To confirm this hypothesis, the $YBCO^{PLD}/YBO^{CSD}/LAO$ sample was studied with electron microscopy.

From the SEM analysis (Fig. 2b and c), it can be seen that no secondary phases are present at the YBCO surface and its microstructure is similar as previously reported by Hühne et al. [20]. Compared to the $YBiO_3$ film prior to YBCO deposition (Fig. 2a), a clear change in morphology and a reduction in both thickness and homogeneity is observed. To investigate the buffer layer – YBCO interface, a cross-sectional lamella was prepared for TEM measurements.

The bright field TEM image confirms that the buffer layer is less uniform than before the YBCO deposition. Overall, the buffer layer thickness decreased and at some points the buffer layer is completely gone. Despite this reduction in thickness, a sharp interface is maintained between the remaining buffer and superconducting material, indicating that no chemical reaction occurred during the YBCO deposition. The reduction in thickness confirms the loss of bismuth throughout the deposition process, leaving an Y_2O_3 layer between the YBCO and the LAO substrate. Given the sublimation sensitivity of bismuth containing compounds, it is likely that $YBiO_3$ decomposes during the deposition process at high temperatures and low pressures, giving rise to the subsequent sublimation of Bi_2O_3 while Y_2O_3 remains as a thin film. It is interesting to note that the remaining Y_2O_3 exhibits the body centered cubic crystal

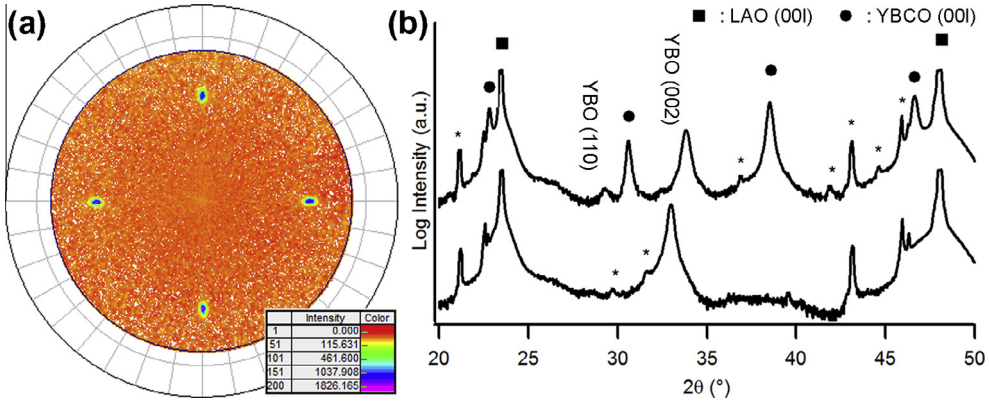

Fig. 1. (a) YBCO (1 0 2) pole figure and (b) XRD analysis of $YBCO^{PLD}/YBO^{CSD}$/LAO prior (bottom) and post (top) YBCO deposition (reflections indexed with an * originate form secondary X-ray radiation).

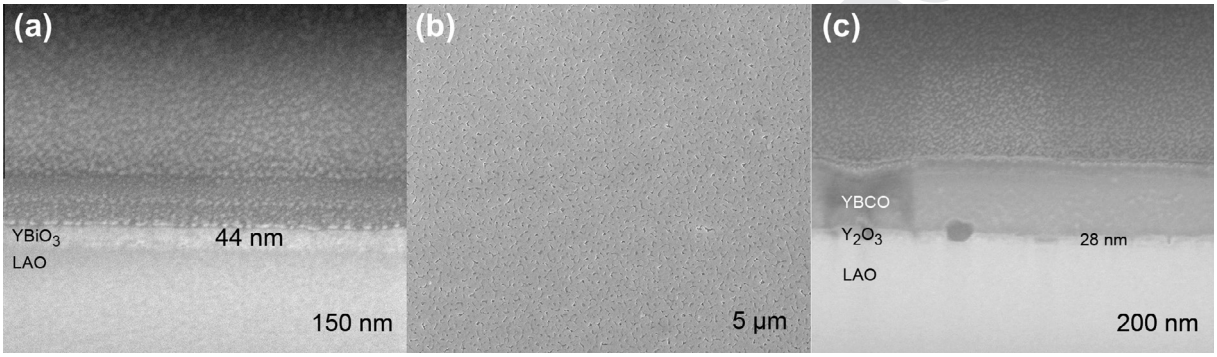

Fig. 2. (a) Cross sectional SEM analysis of the $YBiO_3$ thin film prior to YBCO deposition. (b) Topographical and (c) cross-sectional SEM image of the YBCO film grown by PLD on top of $YBiO_3$-buffered $LaAlO_3$.

structure and the orientation relationship towards the substrate and the YBCO is maintained. This can be deduced from both the bright field and the high resolution TEM images shown in Fig. 3. In bright field, Moiré fringes are clearly visible around the Y_2O_3/YBCO interface. Moiré fringes can originate from two types of small misorientation which causes lattice fringes to overlap: on one hand, a small difference in lattice parameter gives rise to translational Moiré contrast which creates regularly spaced fringes parallel to the lattice plane of investigation, but with a different periodicity. On the other hand, when identical lattices exhibit a small rotational misorientation, rotational Moiré fringes are created, hereby forming fringes perpendicular to the viewed lattice plane. When two materials exhibit both rotational misorientation as well as lattice mismatch, the combination of both fringes results in fringes with different lengths and rotations.

For the YBCO/Y_2O_3/LAO architecture, multiple regions showing Moiré contrast are present. At the Y_2O_3/YBCO interface, this contrast originates from both rotational and translational misfit between overlapping YBCO and Y_2O_3 grains in the viewing direction (marked with C in Fig. 3a–c). In the YBCO film, a lot of strained regions can be observed which deviate from the ideal (00l)-orientation, as well as rotationally misaligned grains causing perpendicular Moiré fringes. This is most likely caused by the microstructural changes of the buffer layer during deposition, causing a larger interface roughness which leads to a higher amount of local defects in the YBCO films. From Fig. 3b, it can be seen that the YBCO is much more defect free in regions where the buffer layer remains flat. The fast Fourier transform of the high resolution image of the buffer layer can be indexed as the[1–10] zone axis of body centered cubic Y_2O_3, meaning that the Y_2O_3 crystal is rotated over 45° in order to decrease the lattice mismatch with the $LaAlO_3$ substrate. Despite the compositional changes, the buffer layer maintains the $(001)_{YBCO}||(001)_{Y2O3}||(001)_{LAO}$ and $[100]_{YBCO}||[110]_{Y2O3}||[100]_{LAO}$ orientation relationship.

The loss of bismuth is further confirmed by BFSTEM–EDX, as shown in Fig. 4. No bismuth containing compounds are found throughout the YBCO layer, indicating complete sublimation of Bi_2O_3 out of the architecture. Despite the excellent superconducting properties, these findings therefore imply that $YBiO_3$ is not a suitable buffer layer candidate for PLD-YBCO deposition.

3.2. Low Fluorine Metalorganic Deposition

The instability of $YBiO_3$ in vacuum conditions at high temperatures limits the use of this material for Pulsed Laser Deposition purposes. As TFA-based YBCO deposition uses conditions similar to those of the $YBiO_3$ synthesis, the vacuum instability is not likely to cause any problems. Therefore, YBCO films were grown on the buffered substrate using different crystallization temperatures.

From the XRD analysis shown in Fig. 5, it is clear that strongly textured YBCO is formed, accompanied by the presence of secondary phases for the films grown at lower temperatures. The films grown at 820 °C exhibit (001) reflections of YBCO only, indicating excellent epitaxial growth. The absence of secondary phases for this sample leads to a T_c of 89.5 K and a critical current density of 1.2 MA/cm^2, whereas the films sintered at lower temperatures exhibit poor superconducting properties. However, for all samples the (002) reflection of $YBiO_3$ is absent, again suggesting the instability of the $YBiO_3$ buffer layer. The secondary phases present at 780 and 810 °C can be identified as YBa_2BiO_6, meaning that barium

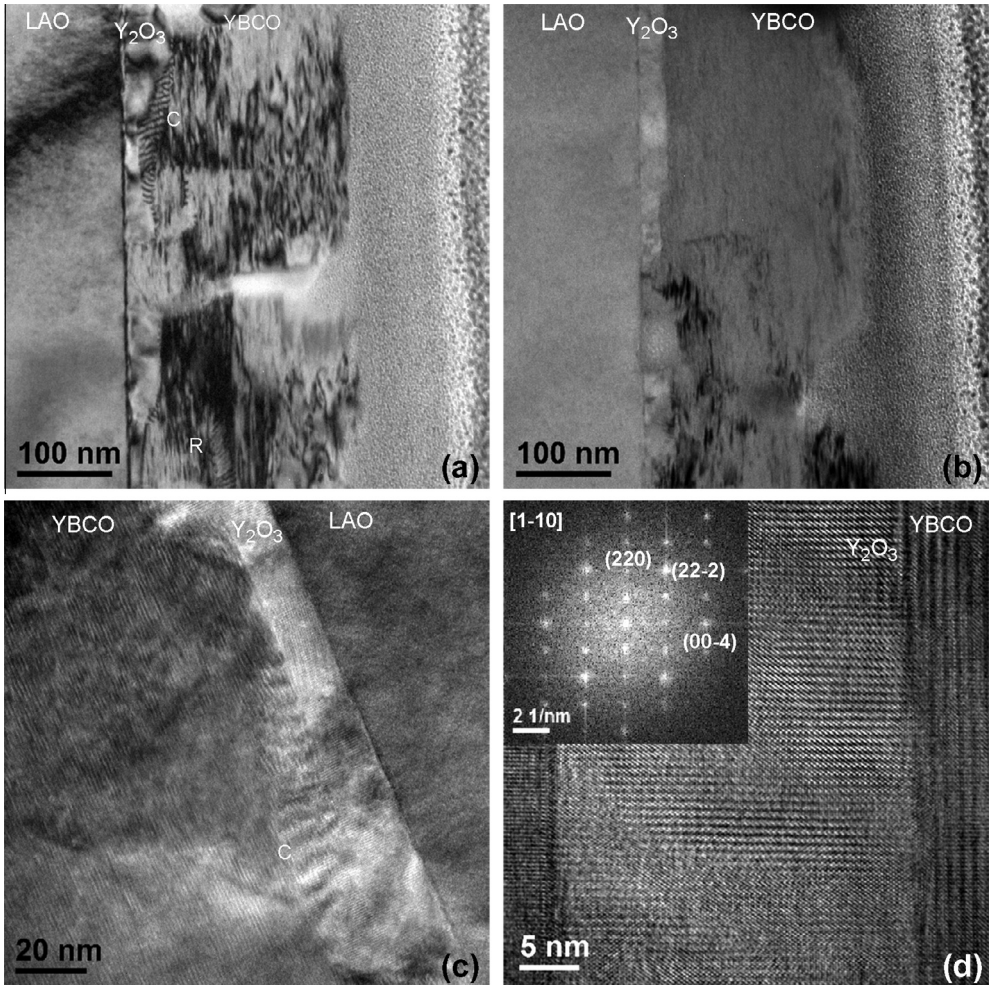

Fig. 3. (a–c) BFTEM ($g = (002)$) overview of YBCO/Y2O3/LAO architecture showing Moiré contrast at the Y_2O_3/YBCO interface and (slightly) misaligned regions in the YBCO film. Combinational or rotational Moiré fringes are indicated by respectively C and R. (d) Average background ZLP-filtered HRTEM image of the LAO/Y_2O_3/YBCO interfaces (Inset: FFT of Y_2O_3 buffer layer).

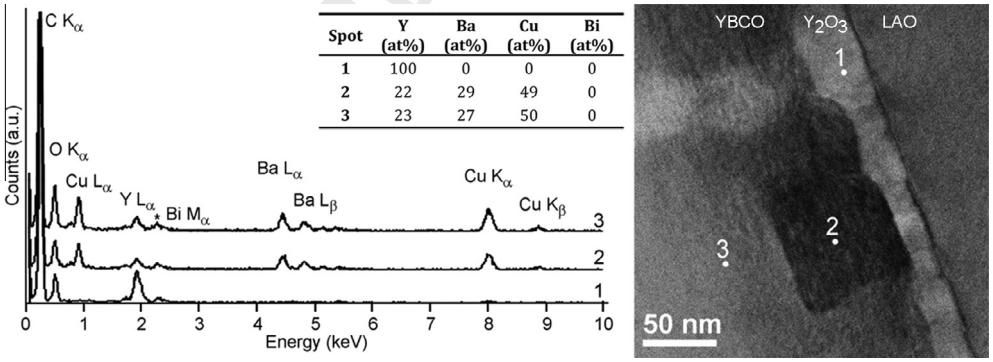

Spot	Y (at%)	Ba (at%)	Cu (at%)	Bi (at%)
1	100	0	0	0
2	22	29	49	0
3	23	27	50	0

Fig. 4. STEM-EDX analysis of YBCO/Y_2O_3/LAO architecture (Peak marked with an * originates from stray radiation of the molybdenum grid).

reacts with the complete buffer layer. At 820 °C no reflections of this compound are present, which most likely can be attributed to the decomposition of YBa_2BiO_6 and subsequent sublimation of bismuth at this temperature.

The microstructural analysis of the different YBCO films is shown in Fig. 6. All films exhibit the typical YBCO topographical structure, but the films grown at 780 °C and 810 °C show the presence of additional phases at the surface of the film. These secondary phases were further analyzed by EDX, which revealed that these compounds mainly consist of Ba, Bi and Y, which is consistent with the detected YBa_2BiO_6 in the XRD analysis. Although some *a*-axis oriented grains are present at the surface of the YBCO films grown at 820 °C, they show a good surface morphology and no bismuth-containing secondary phases are found on the surface.

To study the cross-sectional microstructure of the obtained thin films, TEM-lamellae were produced by FIB and studied with HAADF-STEM and EDX. As can be expected from the SEM and

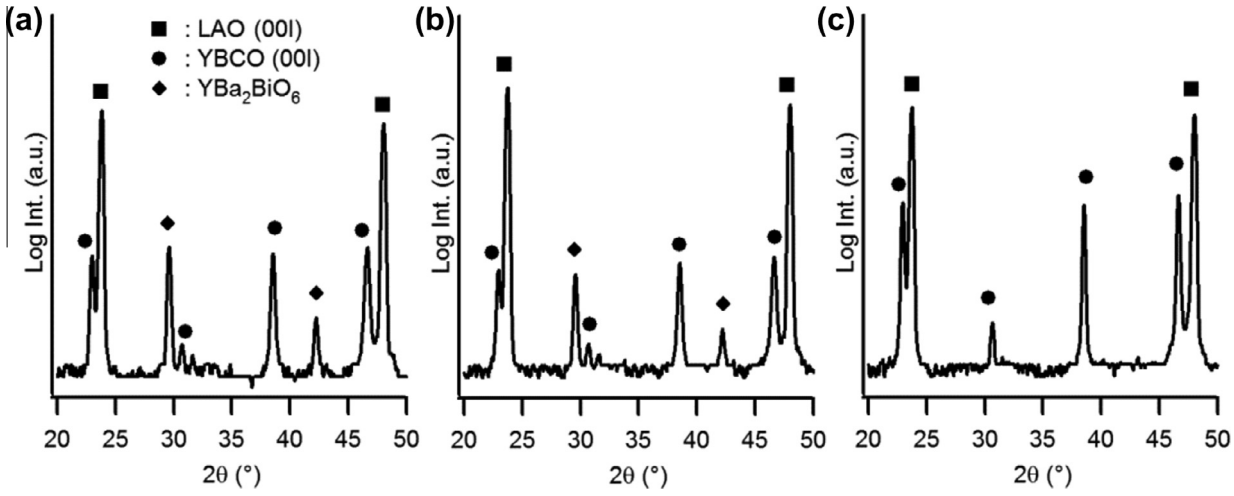

Fig. 5. XRD analysis of YBCO films grown on YBO-buffered LAO at (a) 780 °C, (b) 810 °C, (c) 820 °C.

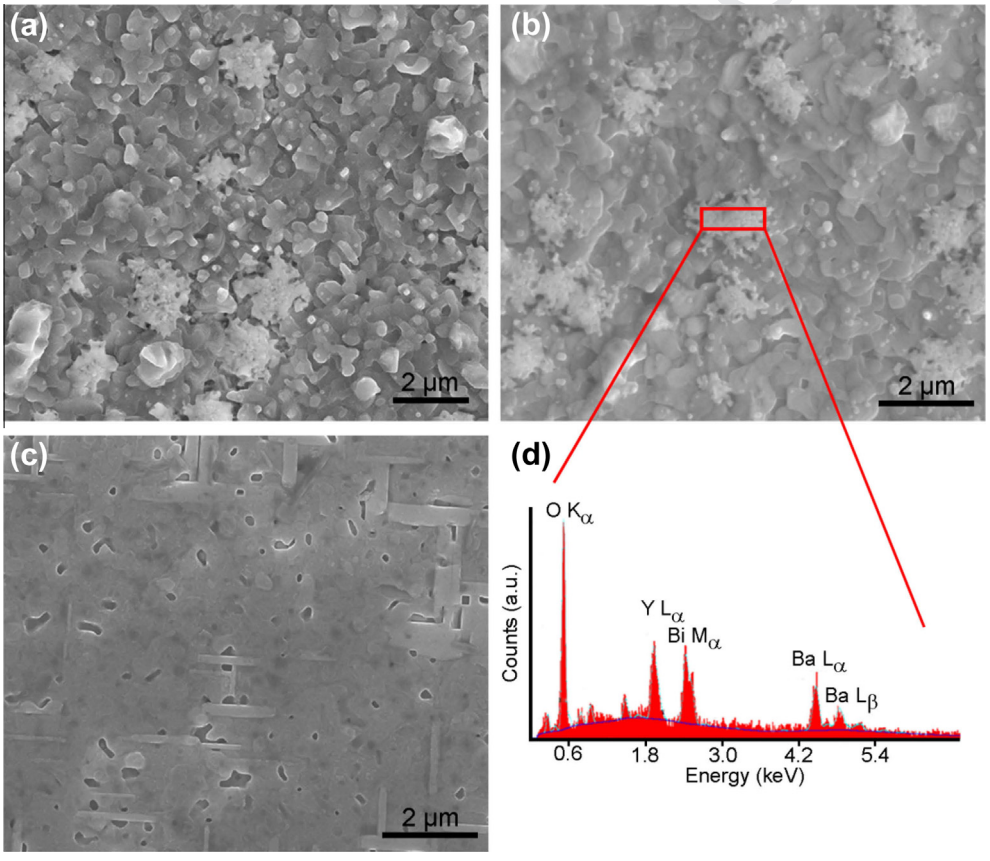

Fig. 6. Topographical SEM analysis of YBCO films grown on YBO buffered LAO at (a) 780 °C, (b) 810 °C, (c) 820 °C and (d) EDX analysis of secondary phases present at YBCO surface indicated by the square in (b). (For interpretation of the references to color in this figure legend, the reader is referred to the web version of this article.)

XRD analysis, a similar microstructure is obtained for the YBCO films grown at 780 and 810 °C. For both samples, it can be seen in Fig. 7 that YBa_2BiO_6 is not present as an intermediate layer between YBCO and the LAO substrate, but large grains of this phase can be found starting from the substrate interface up to the surface of the YBCO film. The darker particles present within the YBa_2BiO_6 phase can be identified as $Y_2Cu_2O_5$, which is a commonly observed intermediate phase during the growth of fluorine-based YBCO films [21–23].

As barium reacts with the $YBiO_3$ buffer layer, the excess of yttrium-cuprate remains present as submicron-sized particles throughout the complete film. Additionally, it can be seen in the HAADF images that the YBCO grains closest to the interface appear brighter. This is not originating from a change in composition, but from electron channeling effects caused by the perfect alignment of these YBCO grains with the single crystal LAO substrate, viewed along the [1 0 0] zone-axis [24]. However, due to the large YBa_2BiO_6 grains present throughout the layer, the epitaxial growth of the

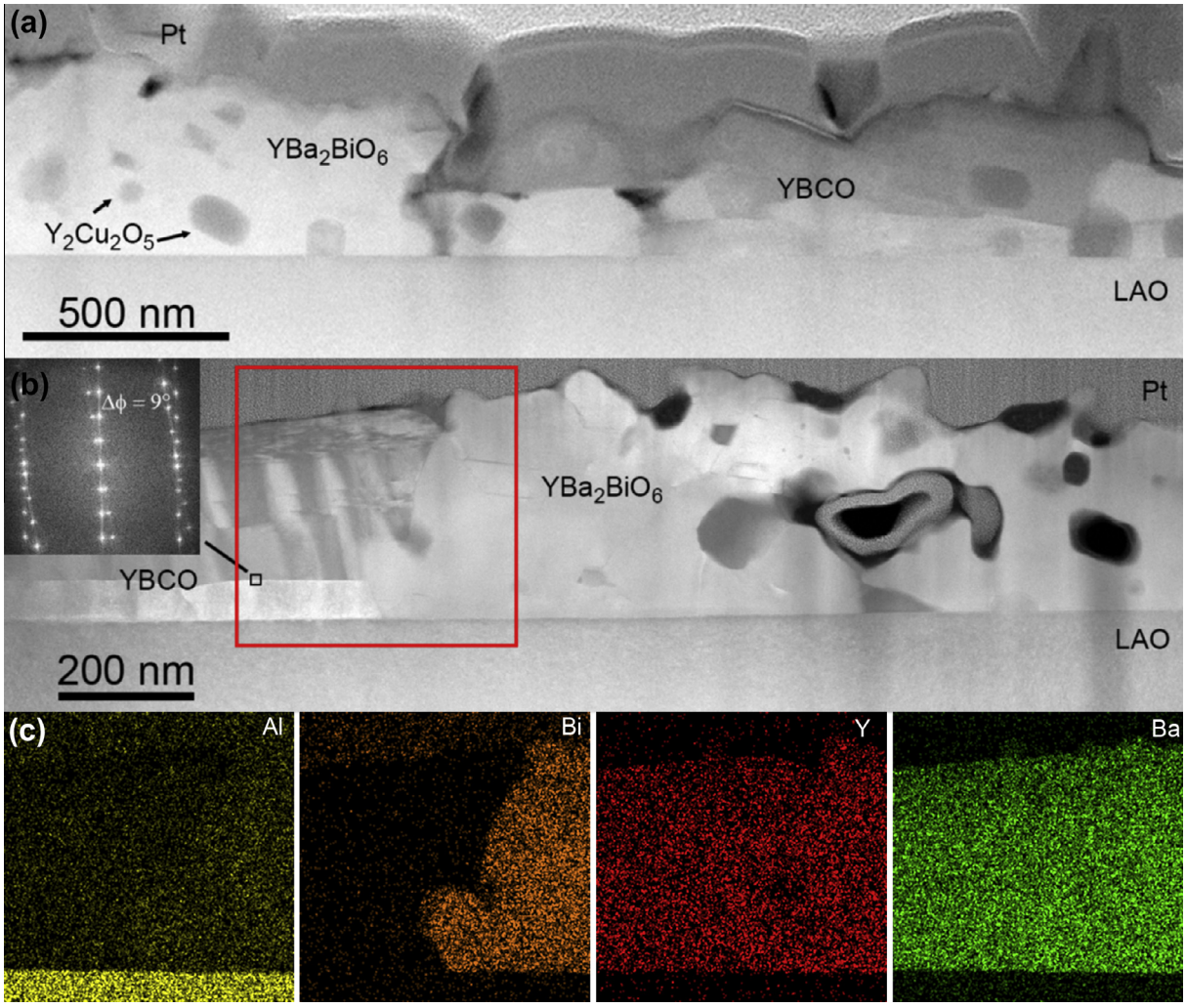

Fig. 7. HAADF-STEM overview of YBCO films grown on $YBiO_3$-buffered LAO substrates at (a) 780 °C and (b) 810 °C (Inset: FFT of YBCO-YBCO grain boundary showing a 9° misalignment). (c) STEM-EDX maps of Al, Bi, Y and Ba from the region shown in (b). (For interpretation of the references to color in this figure legend, the reader is referred to the web version of this article.)

YBCO is disturbed, leading to more weakly (001)-textured YBCO grains towards the surface of the films. Similar columnar-like electron channeling contrast is again observed in these YBCO grains, which is related to the presence of different twin orientations as shown in the bright-field TEM ($g = (020)$) image in the Supporting information.

From the high resolution images in Fig. 8a, it is clear that epitaxial YBCO grains directly nucleated and grew onto the LAO substrate without the presence of any intermediate $YBiO_3$ or Y_2O_3 layer, from which it can be concluded that the whole buffer layer reacts with the available barium during the thermal processing of the YBCO film. Next to the YBa_2BiO_6 formation, the barium deficiency in the YBCO film and the strain caused by the secondary phase gives rise to intergrowths of $YBa_2Cu_4O_8$ (Y124) and $Y_2Ba_4Cu_7O_{15}$ (Y247), which can be considered as two YBCO crystals with an additional CuO plane in between. The YBa_2BiO_6 secondary phase grows polycrystalline and no orientation relationship between YBa_2BiO_6 and LAO or YBa_2BiO_6 and YBCO could be found. From the weak epitaxial growth of YBCO in combination with the current-blocking behavior of the large YBa_2BiO_6 grains, it is clear that poor superconducting performances are obtained for the films grown at 780 and 810 °C. For the YBCO films grown at 820 °C, no more bismuth-containing compounds are present in the layer, hereby confirming the decomposition of YBa_2BiO_6 and subsequent sublimation of Bi_2O_3. Due to the decomposition and the pushing of the secondary phases towards the surface, small amounts of BaO or $Ba(OH)_2$ can occasionally be found at the surface of the YBCO films as shown in the EDX map in Fig. 9. This phenomenon also explains the formation of Y_2O_3 nanocrystallites in the YBCO layer, which are visible in the HAADF overview image and the EDX map.

The YBCO layer is strongly textured and grows epitaxially on the single crystal $LaAlO_3$ substrate, as shown in the high resolution HAADF-STEM images, hereby explaining the good superconducting properties. Again, a similar twin microstructure as for the films sintered at lower temperature is observed, which could indicate that the reaction of YBCO with the buffer layer and the subsequent elevation and decomposition of this secondary phase has an effect on YBCO's microstructure and growth mode.

In order to have a better view on the stability of the buffer layer, a pyrolyzed YBCO film on $YBiO_3$-buffered LAO was studied by TEM. In Fig. 10, the smoothness of the buffer layer is again observed, although some porosity is present, which could not be observed in the SEM analysis. Additionally, the upper part of the buffer layer is found to be randomly oriented, which is consistent with the blurred diffraction spots observed in the previously published RHEED measurements [16]. Most likely, the region used for sample preparation mainly consisted of amorphous surface area where an

Please cite this article in press as: G. Pollefeyt et al., Acta Mater. (2015), http://dx.doi.org/10.1016/j.actamat.2015.08.023

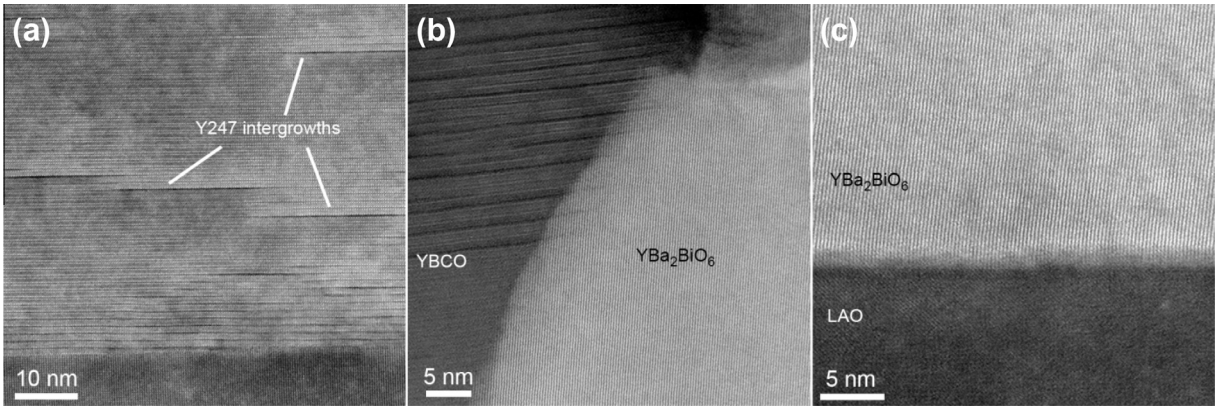

Fig. 8. High resolution HAADF-STEM images of YBCO film grown on $YBiO_3$-buffered LAO at 810 °C: (a) YBCO/LAO interface showing $Y_2Ba_4Cu_7O_{15}$ (Y247) intergrowths in the YBCO layer, (b) YBCO/YBa_2BiO_6 grain boundary, (c) YBa_2BiO_6/LAO interface.

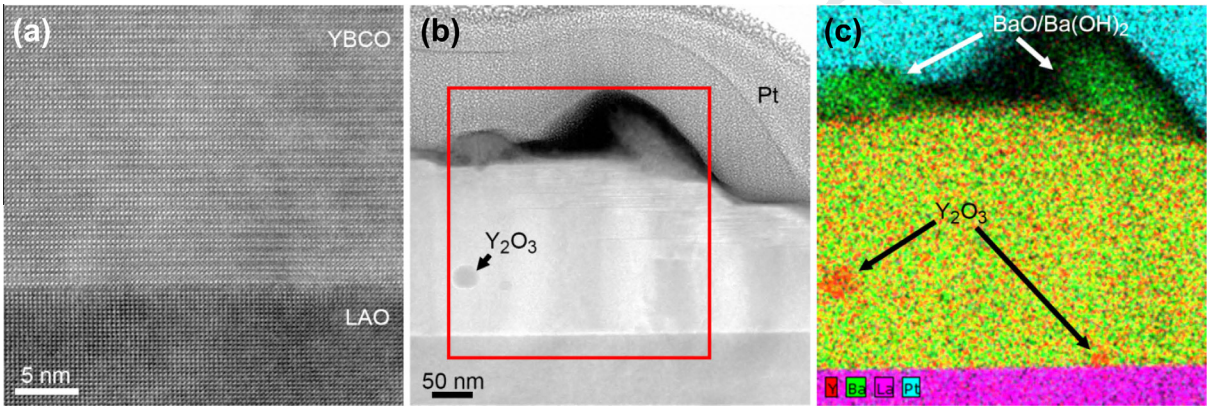

Fig. 9. HAADF-STEM images of YBCO film grown on $YBiO_3$-buffered LAO at 820 °C: (a) High resolution image of YBCO/LAO interface showing direct nucleation of YBCO on the LAO substrate, (b) overview of YBCO film displaying columnar-type of microstructure and secondary phases on top, (c) EDX map of Y (red), Ba (green), La (purple) and Pt (blue) from the region shown in (b). (For interpretation of the references to color in this figure legend, the reader is referred to the web version of this article.)

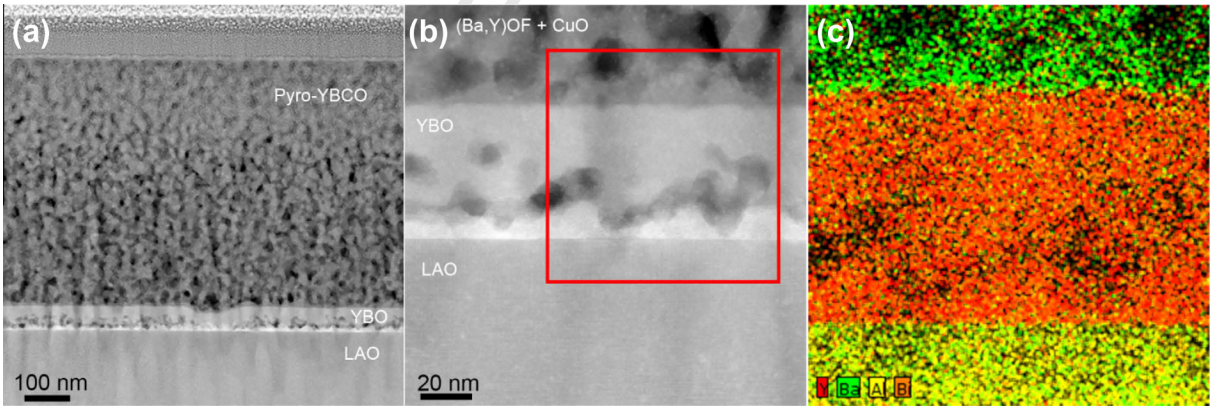

Fig. 10. HAADF-STEM images of low-TFA YBCO film on $YBiO_3$-buffered LAO after pyrolysis at 350 °C in humid oxygen: (a) overview image of YBCO/$YBiO_3$/LAO interface showing the preservation of the buffer layer, (b) overview image of the $YBiO_3$ buffer layer displaying a smooth and reaction-free interface, (c) EDX map of Y (red), Ba (green), Al (yellow) and Bi (orange) from the region shown in (b). (For interpretation of the references to color in this figure legend, the reader is referred to the web version of this article.)

incomplete texturing of the $YBiO_3$ film occurred. Nevertheless, the $YBiO_3$ buffer layer is still chemically intact after pyrolysis, indicating that the reaction of barium with the buffer layer occurs during the crystallization of YBCO, similar to $BaCeO_3$ formation observed for ceria-based buffer architectures [13,25].

Given that within an YBCO formation temperature range of 40 °C, reaction or complete disappearance of the buffer layer is observed, it can be concluded that the $YBiO_3$ buffer layer systems have no advantage over the commonly used and well established CeO_2 cap layer. Therefore, in contradiction to results presented in

literature [17,26,27], it is believed that bismuth-based buffer layers systems are not suitable for implementation in coated conductors.

4. Conclusion

YBO thin films were prepared starting from a water-based precursor solution by dip-coating. The texture transferring properties of YBO were tested by both PLD and TFA-based YBCO deposition on YBO-buffered $LaAlO_3$. Although in both cases good superconducting properties were obtained, respectively 3.6 and 1.2 MA/cm^2, it was shown by an elaborate TEM analysis that the buffer layer is unstable during the YBCO processing. In the case of vacuum deposition, sublimation of bismuth oxide is observed at low pressures and high temperatures, leading to a textured yttria layer which serves as growth template for YBCO. For TFA-based YBCO deposition, reaction of the $YBiO_3$ buffer layer with barium is observed, giving rise to large YBa_2BiO_6 grains which are pushed towards the surface of the YBCO film. When using higher growth temperatures, this secondary phase decomposes and bismuth oxide sublimates out of the complete structure, leaving a textured YBCO film which directly nucleated and grew onto the $LaAlO_3$ single crystal substrate. These results indicate that bismuth-based buffer layers are not suited for replacing CeO_2 in the commonly used buffer-architectures for coated conductors.

Acknowledgements

One of the authors (G.P.) would like to thank the Institute for the Promotion of Innovation through Science and Technology in Flanders (IWT) for funding. Part of this work was performed within the framework of the EuroTapes project (FP7-NMP.2011.2.2-1 Grant No. 280438), funded by the European Union.

Appendix A. Supplementary data

Supplementary data associated with this article can be found, in the online version, at http://dx.doi.org/10.1016/j.actamat.2015.08.023.

References

[1] J. Feys, P. Vermeir, P. Lommens, S.C. Hopkins, X. Granados, B.A. Glowacki, M. Baecker, E. Reich, S. Ricard, B. Holzapfel, P. Van der Voort, I. Van Driessche, Ink-jet printing of $YBa_2Cu_3O_7$ superconducting coatings and patterns from aqueous solutions, J. Mater. Chem. 22 (2012) 3717.
[2] M.P. Siegal, P.G. Clem, J.T. Dawley, R.J. Ong, M.A. Rodriguez, D.L. Overmyer, All solution-chemistry approach for $YBa_2Cu_3O_{7-\delta}$-coated conductors, Appl. Phys. Lett. 80 (2002) 2710.
[3] I. Van Driessche, J. Feys, S.C. Hopkins, P. Lommens, X. Granados, B.A. Glowacki, S. Ricart, B. Holzapfel, M. Vilardell, A. Kirchner, M. Backer, Chemical solution deposition using ink-jet printing for YBCO coated conductors, Supercond. Sci. Technol. 25 (2012) 065017.
[4] X. Obradors, T. Puig, A. Pomar, F. Sandiumenge, N. Mestres, M. Coll, A. Cavallaro, N. Roma, J. Gazquez, J.C. Gonzalez, O. Castano, J. Gutierrez, A. Palau, K. Zalamova, S. Morlens, A. Hassini, M. Gibert, S. Ricart, J.M. Moreto, S. Pinol, D. Isfort, J. Bock, Progress towards all-chemical superconducting $YBa_2Cu_3O_7$-coated conductors, Supercond. Sci. Technol. 19 (2006) S13.
[5] M. Paranthaman, T. Aytug, K. Kim, E.D. Specht, L. Heatherly, Strategic buffer layer development for YBCO coated conductors, IEEE Trans. Appl. Supercond. 19 (2009) 3303.
[6] P. Vermeir, I. Cardinael, M. Backer, J. Schaubroeck, E. Schacht, S. Hoste, I. Van Driessche, Fluorine-free water-based sol-gel deposition of highly epitaxial $YBa_2Cu_3O_{7-\delta}$ films, Supercond. Sci. Technol. 22 (2009) 075009.
[7] J. Kunert, M. Backer, O. Brunkahl, D. Wesolowski, C. Edney, P. Clem, N. Thomas, A. Liersch, Advanced titania buffer layer architectures prepared by chemical solution deposition, Supercond. Sci. Technol. 24 (2011) 085018.
[8] K. Knoth, R. Huhne, S. Oswald, L. Schultz, B. Holzapfel, Detailed investigations on $La_2Zr_2O_7$ buffer layers for YBCO-coated conductors prepared by chemical solution deposition, Acta Mater. 55 (2007) 517.
[9] V. Cloet, T. Thersleff, O. Stadel, S. Hoste, B. Holzapfel, I. Van Driessche, Transmission electron microscopy analysis of a coated conductor produced by chemical deposition methods, Acta Mater. 58 (2010) 1489.
[10] L. Molina, H.Y. Tan, E. Biermans, K.J. Batenburg, J. Verbeeck, S. Bals, G. Van Tendeloo, Barrier efficiency of sponge-like $La_2Zr_2O_7$ buffer layers for YBCO-coated conductors, Supercond. Sci. Technol. 24 (2011) 065019.
[11] V. Cloet, P. Lommens, R. Huhne, K. De Buysser, S. Hoste, I. Van Driessche, A study of the parameters influencing the microstructure of thick $La_2Zr_2O_7$ films, J. Cryst. Growth 325 (2011) 68.
[12] S. Petit, M. Mikolajczyk, J.L. Soubeyroux, T. Waeckerle, R. Batonnet, S. Pairis, P. Odier, LZO, a protective barrier against oxidation of NiW alloys, IEEE Trans. Appl. Supercond. 21 (2011) 2977.
[13] R. Goswami, R.L. Holtz, G. Spanos, Microstructure and interface phase formation in $YBa_2Cu_3O_{7-\delta}$ prepared by an MOD process, IEEE Trans. Appl. Supercond. 17 (2007) 3294.
[14] N. Van-de-Velde, T. Bruggeman, L. Stove, G. Pollefeyt, O. Brunkahl, I. Van-Driessche, Influence of morphology and texture of CeO2 on YBa2Cu3O7 (YBCO) growth and BaCeO3 formation in solution-derived synthesis, Eur. J. Inorg. Chem. (2012) 1186.
[15] X.J. Zhang, W.T. Jin, S.J. Hao, Y. Zhao, H. Zhang, Study of the crystal structures of new buffer materials $Bi_{1-x}Y_xO_{1.5}$, J. Supercond. Nov. Magn. 23 (2010) 1011.
[16] G. Pollefeyt, S. Rottiers, P. Vermeir, P. Lommens, R. Huhne, K. De Buysser, I. Van Driessche, Feasibility study of the synthesis of $YBiO_3$ thin films by aqueous chemical solution deposition as an alternative for CeO2 buffer layers in coated conductors, J. Mater. Chem. A 1 (2013) 3613.
[17] G. Li, M.H. Pu, X.H. Du, Y.B. Zhang, H.M. Zhou, Y. Zhao, A new single buffer layer for YBCO coated conductors prepared by chemical solution deposition, Phys. C 452 (2007) 43.
[18] M. Coll, A. Pomar, T. Puig, X. Obradors, Atomically flat surface: the key issue for solution-derived epitaxial multilayers, Appl. Phys. Express 1 (2008) 085018.
[19] P. Vermeir, F. Deruyck, J. Feys, P. Lommens, J. Schaubroeck, I. Van Driessche, Comments on the wetting behavior of non-porous substrates for ceramic coated-conductor applications, J. Sol-Gel. Sci. Technol. 62 (2012) 378.
[20] R. Huhne, D. Selbmann, J. Eickemeyer, J. Hanisch, B. Holzapfel, Preparation of buffer layer architectures for $YBa_2Cu_3O_{7-x}$ coated conductors based on surface oxidized Ni tapes, Supercond. Sci. Technol. 19 (2006) 169.
[21] X. Obradors, T. Puig, S. Ricart, M. Coll, J. Gazquez, A. Palau, X. Granados, Growth, nanostructure and vortex pinning in superconducting $YBa_2Cu_3O_7$ thin films based on trifluoroacetate solutions, Supercond. Sci. Technol. 25 (2012) 123001.
[22] T. Araki, I. Hirabayashi, Review of a chemical approach to $YBa_2Cu_3O_{7-x}$-coated, superconductors – metalorganic deposition using trifluoroacetates, Supercond. Sci. Technol. 16 (2003) R71.
[23] L.H. Jin, Y.F. Lu, J.Q. Feng, S.N. Zhang, Z.M. Yu, Y. Wang, C.S. Li, Evolution of low fluorine solution in decomposition and crystallization for $YBa_2Cu_3O_y$ film growth, J. Alloy. Compd. 568 (2013) 36.
[24] L. Fitting, S. Thiel, A. Schmehl, J. Mannhart, D.A. Muller, Subtleties in ADF imaging and spatially resolved EELS: A case study of low-angle twist boundaries in $SrTiO_3$, Ultramicroscopy 106 (2006) 1053.
[25] M.P. Paranthaman, S. Sathyamurthy, M.S. Bhuiyan, P.M. Martin, T. Aytug, K. Kim, A. Fayek, K.J. Leonard, J. Li, A. Goyal, T. Kodenkandath, X. Li, W. Zhang, M. W. Rupich, MOD Buffer/YBCO approach to fabricate low-cost second generation HTS wires, IEEE Trans. Appl. Supercond. 17 (2007) 3332.
[26] Y. Zhao, M.H. Pu, G. Li, X.H. Du, H.M. Zhou, Y.B. Zhang, X.S. Yang, Y. Wang, R.P. Sun, C.H. Cheng, Development of a new series of buffer layers for REBCO coated conductors, Phys. C 463 (2007) 574.
[27] Y. Zhao, M.H. Pu, W.T. Wang, M. Lei, C.H. Cheng, H. Zhang, Fabrication and properties of coated conductors with all fluorine-free CSD route, J. Supercond. Nov. Magn. 23 (2010) 971.